Graphane

Deutsche Ausgabe: DOI: 10.1002/ange.201606852
Internationale Ausgabe: DOI: 10.1002/anie.201606852

Graphane Nanostripes

*Lu Wang, Zdeněk Sofer, Daniel Bouša, David Sedmidubský, Štěpán Huber, Stanislava Matějková, Alena Michalcová, and Martin Pumera**

Abstract: *Graphane, the hydrogenated counterpart of graphene, was shown to exhibit properties such as tunable band gaps through varied degrees of hydrogenation, fluorescence, or ferromagnetism. Graphane nanostripe properties have also been theoretically predicted. Herein, we show that graphane nanostripes can be prepared by opening carbon nanotubes using Birch reduction in liquid ammonia utilizing potassium as a reducing agent and water as a proton donor. The prepared graphane nanostripes exhibit several exceptional properties when coupled with trace metal dopants. The interplay of metallic nanoparticles and defects lead to a spin polarization and induction of ferromagnetic moment, as well as to enhanced electrocatalytic properties in the hydrogen evolution reaction when compared to non-hydrogenated carbon nanotubes.*

Hydrogenated graphene (graphane) is an important graphene derivate. Its structure is based on graphene, a single sheet of carbon atoms arranged in a hexagonal honeycomb-like pattern.[1] In graphene, the carbon atoms are in an sp^2 hybridization imposed by the trigonal planar arrangement of nearest neighbors. In contrast, graphane is a reduced form of graphene, with four bonds from each sp^3-hybridized carbon, three of which provide links to neighboring carbon atoms and one to hydrogen. The schematic drawing of synthesis procedure is shown in Figure 1. Graphane exhibits many different properties from graphene: it is a semiconductor with a band gap of 3.7 eV, it exhibits fluorescence, and, if partly hydrogenated, it exhibits ferromagnetism.[2] Various methods have been used for hydrogenated graphene fabrication, such as low pressure H_2 plasma hydrogenation, high pressure hydrogenation, or wet-chemistry Birch reactions. The resulting hydrogenated graphenes showed coverage of the carbon sheets by hydrogen ranging from 3 to 10% by low pressure plasma hydrogenation,[3] and close to 100% by wet-chemistry methods.[4]

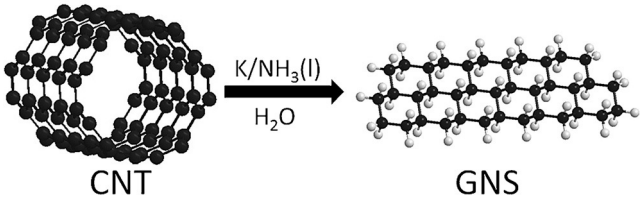

Figure 1. Graphane nanostripes synthesis by carbon nanotube opening and hydrogenation.

Graphane nanostripes have been theoretically predicted and discussed in the literature.[5] Moreover, their synthesis has been proposed based on the hydrogenation of carbon (sp^2) nanotubes, and the band gap of the resulting nanomaterials has been predicted to be controlled by tuning the hydrogenation level. In this study, we prepared and characterized hydrogenated carbon nanostripes (graphane nanostripes). We show that the presence of metallic nanoparticles leads to induction of ferromagnetism within the graphane nanostripes. Graphane nanostripes decorated by metallic nanoparticles are also highly efficient hybrid electrocatalysts for hydrogen evolution and oxygen reduction reaction.

The hydrogenated graphane nanostripes (GNSs) were synthesized through wet-chemistry Birch reduction of carbon nanotubes (CNTs). We used metallic potassium (in liquid ammonia) as a reducing agent and water as a proton donor during the reduction. The resulting hydrogenated carbon nanotubes were characterized by X-ray photoelectron spectroscopy (XPS), elemental combustion analysis, Raman spectroscopy, magnetometry, and finally the electrochemical properties toward oxygen reduction reaction (ORR), hydrogen evolution reaction (HER), and their capacitive behavior were studied.

The structure and morphology of GNSs were investigated by SEM and TEM microscopy (Figure 2a and 2b). The morphology of GNSs indicated a high degree of disorder and large mass of stacked nanostripes, however few damaged carbon nanotubes were found in the material. The TEM image (Figure 2b) indicated the presence of cobalt nanoparticles, which induce the ferromagnetic ordering. Their presence is discussed below. The TEM images (Figure 2c and 2d) demonstrated that the Birch hydrogenation procedure also led to CNT opening and formation of stripes. The opening of CNTs allowed a significantly higher degree of hydrogenation compared to closed and only surface hydrogenated nanotubes, as graphene stripes display accessible sides as well as edges where each C atom is hydrogenated with

[*] Dr. L. Wang, Prof. Dr. M. Pumera
Division of Chemistry and Biological Chemistry
School of Physical and Mathematical Sciences
Nanyang Technological University
Singapore 637371 (Singapore)
E-mail: pumera@ntu.edu.sg
Prof. Dr. Z. Sofer, D. Bouša, Prof. Dr. D. Sedmidubský, Dr. Š. Huber
Department of Inorganic Chemistry
University of Chemistry and Technology Prague
Technická 5, 166 28 Prague 6 (Czech Republic)
Dr. S. Matějková
Institute of Organic Chemistry and Biochemistry, v.v.i.
Flemingovo Nám. 12, Prague 6 (Czech Republic)
Dr. A. Michalcová
Department of Metals and Corrosion Engineering
University of Chemistry and Technology Prague
Technická 5, 166 28 Prague 6 (Czech Republic)

Supporting information for this article can be found under: http://dx.doi.org/10.1002/anie.201606852.

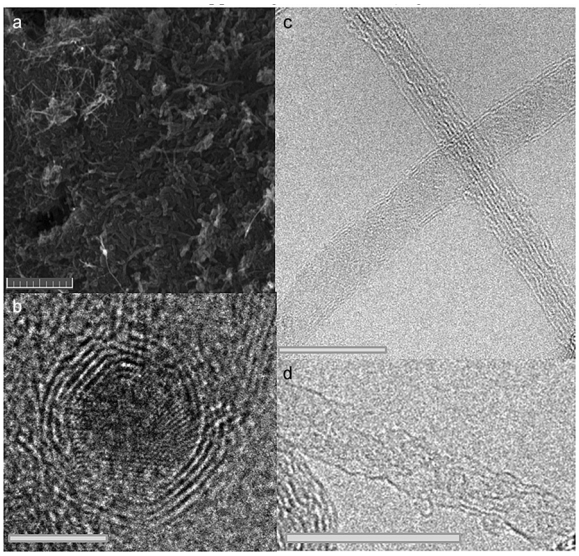

Figure 2. a) SEM image of graphane nanostripes. Scale bar = 500 nm. b) TEM image of cobalt nanoparticle in GNSs. Scale bar = 5 nm. c, d) TEM images of GNSs. Scale bars = 30 nm and 15 nm, respectively.

two H atoms. The width of the GNSs were about 10–20 nm. The opening of CNTs was associated with a suppression of metallic impurities concentration, however the metallic particles were still present and composed predominantly of cobalt (Figure 2b), which was detected by ICP-OES as the dominant impurity. These particles were coated by several layers of carbon, clearly visible on the TEM images. The STEM image with corresponding EDS map is shown in the Supporting Information (Figure S1). The EDS analysis performed in addition to ICP-OES is discussed below. The measurement showed the presence of 93.2 wt% C and 4.0 wt% of O. In addition, several impurities such as Co (0.7 wt%), K (1.5 wt%), Cl (0.5 wt%), Si (0.1 wt%), and S (0.1 wt%) were identified. Potassium and chlorine originated from the hydrogenation procedure, while the cobalt nanoparticles originated from the parent carbon nanotubes, where Co was the main catalyst component used in the chemical vapor deposition (CVD) method for CNT growth. For comparison, the morphology of carbon nanotubes obtained by SEM and TEM is shown in the Supporting Information (Figure S2).

Combustible elemental analysis was used to determine the elemental composition of the CNTs and GNSs. This method is useful to measure the absolute content of the C, H, N, and O elements in the material (the concentration of O is estimated indirectly from the mass difference). In combination with XPS, it provides further insight into the composition and character of chemical bonding in the samples. We found that the hydrogenation rate of carbon nanotubes reached 40% (Table 1), yielding a composition of $C_{2.6}H_1$. Provided that in carbon nanotubes, unlike graphene, hydrogenation can only take place on the outer surface (for closed CNTs), the hydrogenation limit for few layer nanotubes is only a small percent (for example, 10 atom% for 5-walled CNT). However, the relatively high concentration of hydrogen indicates the opening of carbon nanotubes and formation of graphane

Table 1: Elemental combustion analysis of graphane nanostripes (GNS) and as-received carbon nanotubes (CNT).

Sample	Treatment	At% N	At% C	At% H	At% O
CNT	none	0.12	94.23	0.60	5.04
GNS	$K/NH_3/H_2O$	0.49	67.41	26.31	5.78

nanostripes. The effect of carbon nanotubes opening and formation of graphane nanostripes was also observed in the TEM images.

X-ray photoelectron spectroscopy was employed to investigate the elemental composition and bonding information of the CNTs. XPS is a chemical analysis method and it is useful not only to determine the elemental composition of the sample but also the valency and bonding arrangement of the involved atoms. The wide scan and C1s high-resolution XPS of CNTs are shown in Figure 3. The peak at 450 eV originates

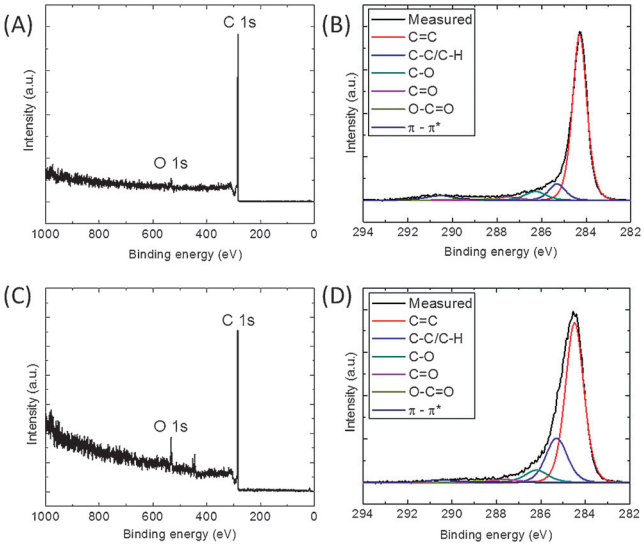

Figure 3. Wide-scan XPS of: A) CNTs and C) GNSs. High-resolution C1s of: B) CNTs and D) GNSs.

from indium sample holder. The high-resolution XPS of the C1s signal provides insight into the chemical composition of the residual oxygen-containing groups, as they show different energy levels: C=C bonds of 284.5 eV, C–C/C–H bond of 285.6 eV, C–O bond of 286.6 eV, C=O bond of 287.6 eV, O–C=O bond of 289.6 eV, and π-π interactions of 291.2 eV. The detailed bonding information of CNTs and GNSs is shown in Table 2. Clearly, the C–C/C–H bond is much more frequent in hydrogenated samples, indicating (together with the elemental analysis) successful opening and hydrogenation of the carbon nanotubes.

Table 2: Bonding information (%) of CNTs and GNSs.

	C=C [%]	C–C/C–H [%]	C–O [%]	C=O [%]	O–C=O [%]	π-π* [%]
CNT	74.2	8.6	6.1	2.6	3.6	4.8
GNS	65.8	21.3	6.7	2.2	1.8	2.2

The defect density and formation of sp^3-hybridized carbon atoms in GNSs were studied by Raman spectroscopy (Figure 4). The *D* band at approximately 1350 cm^{-1} is associated with sp^3-hybridized carbon atoms and defects within the carbon atom plane, while the pristine lattice of sp^2-

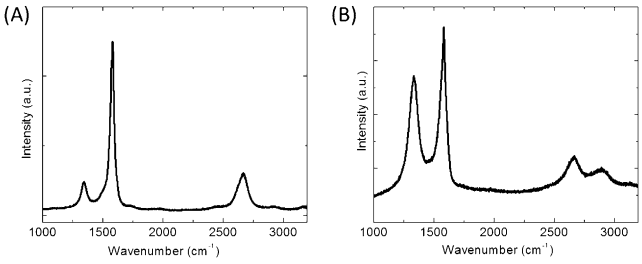

Figure 4. Raman spectra of A) CNTs and B) GNSs.

bonded carbon atoms in the graphene sheet shows a *G* band at approximately 1560 cm^{-1}. The ratio between *D* and *G* band intensities (I_D/I_G) can be used as an indication of the degree of disorder and sp^3-hybridized carbon atoms within the structure. The I_D/I_G ratios 0.174 and 0.711 were found for CNTs and GNSs, respectively. After hydrogenation, a significant amount of sp^3-hybridized carbon atoms are formed, indicating the formation of graphane nanostripes.

To confirm of the presence of C–H bonds in graphane nanostripes, FT-IR spectroscopy was performed. Two absorption bands at 2850 cm^{-1} and 2920 cm^{-1} were clearly visible (Figure 5). The stronger absorption band at 2850 cm^{-1} originates from C–H bonds within the plane of the GNSs, while the absorption band at 2920 cm^{-1} results from $C–H_2$ groups on the edges of the GNSs. In addition, the very weak absorption band at 2990 cm^{-1} could be attributed to methyl groups ($C–H_3$) formed on the edges of the GNSs owing to the violent opening and hydrogenation conditions.

The transition metal impurities were identified by ICP-OES using an electrothermal vaporization system (ETV) and

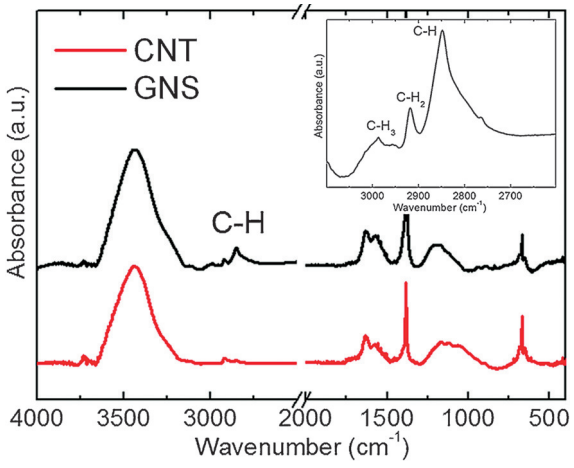

Figure 5. The FT-IR spectra of CNT before and after hydrogenation/opening procedure (GNSs). The inset shows the details of the C–H bond spectral region.

Table 3: The composition obtained by ICP-OES (ppm).

Element	CNT	GNS
Al	18.8	37.8
B	0.00	0.00
Ba	4.50	1.40
Ca	3315	538
Cd	3.50	11.8
Co	5072	2200
Cr	95.1	40.2
Cu	0.20	5.70
Fe	324.0	110.6
Mg	635.0	99.0
Mn	5.40	4.40
Ni	40.4	4.10
Pb	6.00	5.20
Zn	1.90	3.20
Mo	1269	0.00

wet-digestion methods. The knowledge of exact impurity concentrations is critical for detailed investigations of the magnetic properties and electrocatalytic activity. To interpret the magnetic behavior, the exact content of magnetically active elements such as Fe, Co, Ni, and Mn is essential. The concentrations of impurities obtained by ICP-OES for the starting CNTs, as well as for the formed graphane nanostripes are summarized in Table 3. A significant suppression of metallic impurities concentration was observed after hydrogenation originating from the opening of carbon nanotubes, which led to easier removal of nanoparticles by washing after hydrogenation. The most significant changes were observed for cobalt, iron, molybdenum, and nickel, as well as for some other non-catalytic impurities such as Ca and Mg.

In particular, considering its content and magnetic moment, cobalt has a substantial influence on the resulting magnetic properties of both the original material and graphane nanostripes. As seen in Figure 6b, the magnetic moment of CNTs display a saturation at 1.49 μ_B per Co at 300 K, corresponding to a ferromagnetic moment falling in the range between bulk and nanoscopic cobalt. At low temperatures, a clear paramagnetic component is superimposed on the saturated ferromagnetic moment that is slightly enhanced ($+0.08\ \mu_B$) compared to room temperature. The Brillouin fit applied on the low-temperature data after subtracting the FM part yielded a paramagnetic spin $S = 0.5$/Co and a critical temperature close to 0 K ($+0.5$ K). The localized paramagnetic moments can be attributed to a highly disordered and possibly oxidized surface of Co-nanoparticles. This scenario is also supported by the fact that the same value of paramagnetic moment per Co atom was obtained for the hydrogenated sample with much lower Co content (see Table 3).

Surprisingly, the saturated ferromagnetic moment for graphane nanostripes (2.8 and 2.95 μ_B/Co for 300 and 4.5 K, respectively; Figure 6a) notably exceeds that of the parent material and even that of bulk Co. Such exotic behavior can be interpreted in terms of additional spin-polarized and highly degenerate charge carriers within the GNS matrix, apparently associated with defects brought about by hydrogenation and C–H bond formation and experiencing an effective field of Co nanoparticles cores.

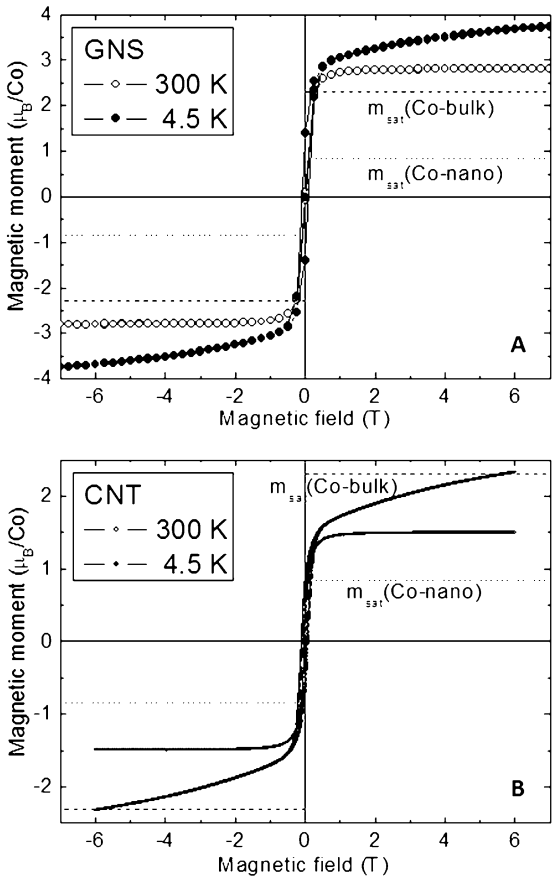

Figure 6. Magnetization curves of graphane nanostripes (Figure 5a) and carbon nanotubes (Figure 5b). All of the data are corrected for carbon core diamagnetism.

Before investigating the electrocatalytic properties of hydrogenated carbon nanotubes, the amount of trace metals in the carbon nanotubes remaining there from their synthesis[6] was carefully analyzed in both the starting CNTs and the hydrogenated GNSs, as they exhibit a pronounced catalytic effect in many electrochemical reactions. ICP/OES measurements were performed to obtain detailed information about the metals present in the samples (Table 3). Interestingly, the results suggest that Mo-based impurities were completely removed, and after hydrogenation the sample showed a higher level of purity than the parent CNTs. This originates from CNT opening and subsequent exposing of the nanoparticles to the surrounding environment.

Next, we investigated the catalytic performance of the GNSs in the oxygen reduction reaction. The reduction of oxygen was recorded on a bare glassy carbon (GC) electrode, CNTs-pure (CNTs without any metallic impurities,[7] CNTs, and GNSs as shown in Figure 7. Both the bare GC electrode and the CNTs-pure exhibited a similar reduction wave with the onset potentials of −273 mV (vs. Ag/AgCl) and −302 mV, respectively. The oxygen reduction with CNTs and GNSs occurred at much lower potentials of −153 mV and −146 mV, respectively, indicating a strong electrocatalytic effect that originates from the doping metal. The high similarity in catalytic behavior of CNTs and hydrogenated GNSs arises from the fact that, unlike Mn and other TM-based nano-

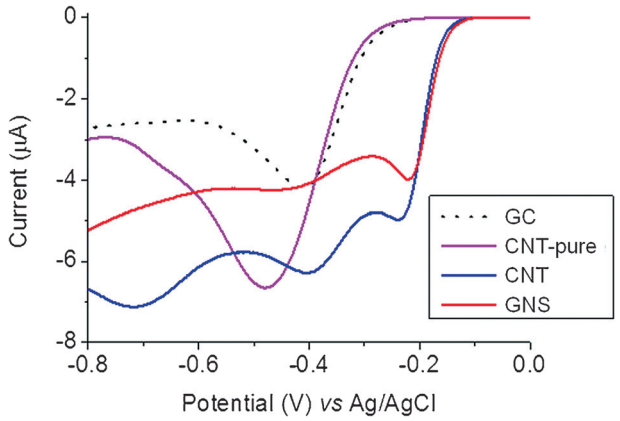

Figure 7. Linear sweep voltammogram of ORR at bare GC, CNT-pure, CNTs, and GNSs, at a scan rate of 10 mV s^{-1} in 0.1 M KOH solution.

particles, carbon does not act as a catalytic site.[8] Hydrogenation of CNTs thus does not play any role in the way the reaction is catalyzed.

Subsequently, we focused on another important electrochemical reaction, the hydrogen evolution reaction. This reaction is highly surface dependent, involving: i) adsorption of a proton on the surface, its reduction to surface-bonded hydrogen (Volmer step), and either ii) recombination with yet another surface-bonded hydrogen (Tafel step), or iii) recombination with a proton in the solution in a simultaneous reduction (Heyrovsky step). Here, the highly hydrogenated GNS surface exhibited superior catalytic activity over the non-hydrogenated CNTs. In detail, linear sweep voltammetry was employed to study the electrochemical performance towards HER (Figure 8). Bare GC electrode and CNTs-pure exhibited similar electrochemical behaviors toward HER and produced more negative reduction potentials than both CNTs and GNSs. The overpotential at the current density of −10 mA cm^{-2} for bare GC electrode, CNTs-pure, CNTs, and GNSs were 0.96 V (vs. RHE), 0.77 V, 0.71 V, and 0.56 V, respectively. The Tafel slopes for all of the samples were calculated to be 157, 106.5, 265.6, and 85.3 for GC, CNTs-pure, CNTs, and GNSs, respectively. However, GNSs show much more positive reduction potentials, even when the amount of metal catalysts is lower than in CNTs. The hydrogen atoms in graphane nanostripes significantly lower the energy barrier of hydrogen reduction. The improvement in the electrocatalytic activity could be explained as a consequence of CNTs opening and exposing electrocatalytic impurities to the environment.

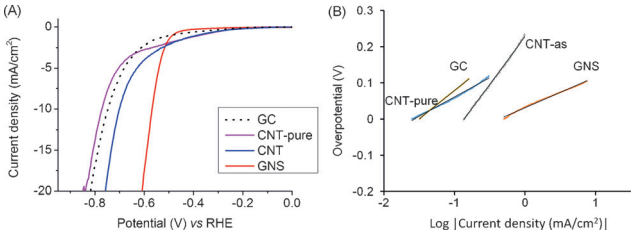

Figure 8. A) Linear sweep voltammogram and B) Tafel plot of HER at bare GC, CNT-pure, CNT, and GNS at scan rate of 2 mV s^{-1} in 0.5 M H_2SO_4 solution.

Table 4: Specific weight capacitance ($F g^{-1}$) of CNTs-pure, CNTs, and GNSs.

Discharge current [$A g^{-1}$]	5.0	2.0	1.0	0.5	0.2	0.1
CNTs-pure	4.89	4.82	5.51	6.39	7.25	9.61
CNTs	60.82	62.39	64.33	67.47	74.44	103.67
GNS	39.21	39.96	41.63	44.44	60.14	69.31

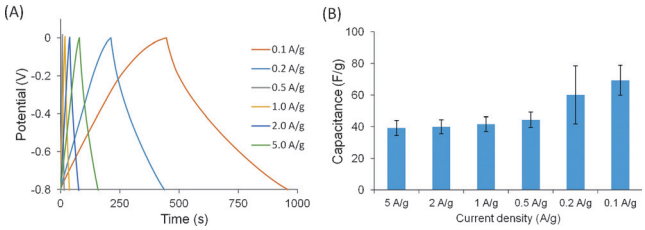

Figure 9. A) Galvanostatic charge/discharge curve of GNS in 6 M KOH solution at different current densities, and B) specific weight capacitance of GNS at different current density.

Moreover, we investigated the specific weight capacitance of GNSs, as determined by galvanostatic charge/discharge curve analysis (Figure 9 and Table 4). The specific weight capacitancies for GNSs were 39.21, 39.96, 41.63, 44.44, 60.14, and 69.37 $F g^{-1}$ at the current densities of 5, 2, 1, 0.5, 0.2, and 0.1 $A g^{-1}$, respectively. Such specific weight capacitance is competitive to some reported CNTs.[9]

We have produced graphane nanostripes through Birch reduction of carbon nanotubes using potassium as an electron source and water as a proton source in liquid ammonia. The hydrogenation was close to the saturation point ($\approx$26 atom %). Graphane nanostripes exhibited high catalytic activity for hydrogen evolution owing to the combination of hydrogenated surfaces facilitating the reaction and cobalt nanoparticles present as impurities in the parent carbon nanotubes. The graphane nanostripes exhibit ferromagnetism significantly exceeding the concentration of all possible magnetic impurities. This effect can be explained in terms of spin-polarized charge carriers trapped on defects and hydrogenated carbon atoms.

Experimental Section

The synthesis of hydrogenated graphene nanostripes (GNSs) was performed using 8 nm multiwall CNTs. The opening and subsequent hydrogenation was performed in liquid ammonia using potassium as an intercalation agent and electron source and water as a proton source. An amount of 250 mg of MW-CNTs was placed together with 8.1 g of K into the reaction vessel and 170 mL of ammonia were condensed on reaction mixture. Water was added in two steps, after 2 hours and 4 hours in 1.9 mL portions. Finally, the reaction mixture was diluted with water and, after evaporation of ammonia, the formed GNSs were separated by suction filtration and repeatedly washed with hydrochloric acid/water (1:1), water, and methanol. GNSs were dried in vacuum oven at 50 °C for 48 hours. More details on the used synthesis methods are given in the Supporting Information.

SEM and STEM microscopy were performed using a Tescan Lyra dual beam microscope. Transmission electron microscopy images were obtained using an EFTEM Jeol 2200 FS microscope (Jeol, Japan). High-resolution X-ray photoelectron spectroscopy (XPS) was performed on an ESCAProbeP spectrometer equipped with a monochromatic aluminum X-ray radiation source (1486.7 eV). The transmittance was measured using a FT-IR spectrometer iS50R (Thermo Scientific, USA). The magnetic properties were measured using Physical Property Measurement System (PPMS) EverCool-II (Quantum Design, USA) using the VSM option. An inVia Renishaw Raman microscope was used for Raman spectroscopy in backscattering geometry (laser 532 nm, 5 mW). Combustible elemental analysis (CHNS-O) was performed using a PE 2400 Series II CHNS/O Analyzer from PerkinElmer. The elemental composition was determined by Inductively Coupled Plasma Optical Emission Spectrometry (ICP-OES) using Spectro ARCOS spectrometer from SPECTRO Analytical Instruments coupled with Electro-Thermal Vaporization (ETV) unit. All of the voltammetric experiments were measured by using an electrochemical analyzer Autolab PGSTAT 101 from Metrohm Autolab. Details for all of the characterization methods are given in the Supporting Information.

Acknowledgements

M.P. was supported by a Tier 2 grant. Z.S., D.B., D.S., and Š.H. were supported by Czech Science Foundation (GACR No. 15-09001S and 16-05167S) and by Specific University Research (MSMT No. 20-SVV/2016). A.M. was supported by Czech Science Foundation (GACR No. P108/12/G043).

Keywords: Birch reduction · capacitance · electrochemistry · graphane nanostripes · magnetism

How to cite: *Angew. Chem. Int. Ed.* **2016**, *55*, 13965–13969
Angew. Chem. **2016**, *128*, 14171–14175

[1] D. C. Elias, R. R. Nair, T. Mohiuddin, S. Morozov, P. Blake, M. Halsall, A. Ferrari, D. Boukhvalov, M. Katsnelson, A. Geim, *Science* **2009**, *323*, 610–613.
[2] M. Pumera, C. H. A. Wong, *Chem. Soc. Rev.* **2013**, *42*, 5987–5995.
[3] J. S. Burgess, B. R. Matis, J. T. Robinson, F. A. Bulat, F. K. Perkins, B. H. Houston, J. W. Baldwin, *Carbon* **2011**, *49*, 4420–4426.
[4] a) A. Y. S. Eng, H. L. Poh, F. Sanek, M. Marysko, S. Matejkova, Z. Sofer, M. Pumera, *ACS Nano* **2013**, *7*, 5930–5939; b) D. Bouša, J. Luxa, D. Sedmidubsky, Š. Huber, O. Jankovský, M. Pumera, Z. Sofer, *RSC Adv.* **2016**, *6*, 6475–6485; c) K. Subrahmanyam, P. Kumar, U. Maitra, A. Govindaraj, K. Hembram, U. V. Waghmare, C. Rao, *Proc. Natl. Acad. Sci. USA* **2011**, *108*, 2674–2677; d) R. A. Schäfer, J. M. Englert, P. Wehrfritz, W. Bauer, F. Hauke, T. Seyller, A. Hirsch, *Angew. Chem. Int. Ed.* **2013**, *52*, 754–757; *Angew. Chem.* **2013**, *125*, 782–786.
[5] L. F. Huang, X. H. Zheng, G. R. Zhang, L. L. Li, Z. Zeng, *J. Phys. Chem. C* **2011**, *115*, 21088–21097.
[6] M. Pumera, *Langmuir* **2007**, *23*, 6453–6458.
[7] T. Kolodiazhnyi, M. Pumera, *Small* **2008**, *4*, 1476–1484.
[8] L. Wang, A. Ambrosi, M. Pumera, *Angew. Chem. Int. Ed.* **2013**, *52*, 13818–13821; *Angew. Chem.* **2013**, *125*, 14063–14066.
[9] a) R. Shah, X. Zhang, S. Talapatra, *Nanotechnology* **2009**, *20*, 395202; b) C. Du, J. Yeh, N. Pan, *Nanotechnology* **2005**, *16*, 350; c) S. Talapatra, S. Kar, S. Pal, R. Vajtai, L. Ci, P. Victor, M. Shaijumon, S. Kaur, O. Nalamasu, P. Ajayan, *Nat. Nanotechnol.* **2006**, *1*, 112–116.

Received: July 14, 2016
Revised: July 29, 2016
Published online: September 7, 2016

